Mon. Not. R. Astron. Soc. **000**, 000–000 (0000) Printed 1 April 2014 (MN LATEX style file v2.2)

An Implementation of Bayesian Lensing Shear Measurement

Erin S. Sheldon⋆
Brookhaven National Laboratory, Bldg 510, Upton, New York 11973

1 April 2014

arXiv:1403.7669v1 [astro-ph.CO] 29 Mar 2014

ABSTRACT

The Bayesian gravitational shear estimation algorithm developed by Bernstein & Armstrong (2014) can potentially be used to overcome noise bias and recover shear using very low signal-to-noise ratio (S/N) galaxy images. In that work the authors confirmed the method is sufficiently unbiased for planned surveys ($\Delta g/g < 2 \times 10^{-3}$) in a simplified demonstration, but no test was performed on images. Here I present a full implementation for fitting models to galaxy images, including the effects of a point spread function (PSF) and pixelization. I tested the implementation using simulated galaxy images modeled as Sérsic profiles with $n = 1$ (exponential) and $n = 4$ (De Vaucouleurs'), convolved with a PSF and a flat pixel response function. I used a round Gaussian model for the PSF to avoid potential PSF-fitting errors. I simulated galaxies with mean *observed, post-PSF* full-width at half maximum equal to approximately 1.2 times that of the PSF, with log-normal scatter. I also drew fluxes from a log-normal distribution. I produced independent simulations, each with pixel noise tuned to produce different mean S/N ranging from $10 - 1000$. I applied a constant shear to all images. I fit the simulated images to a model with the true Sérsic index to avoid modeling biases. I recovered the input shear with fractional error $\Delta g/g < 2 \times 10^{-3}$ in all cases, confirming that, *in these controlled conditions*, the method is sufficiently unbiased for planned surveys.

Key words: cosmology: observations, gravitational lensing: weak, dark energy

1 INTRODUCTION

Noise bias is one of the largest potential systematic errors in weak gravitational shear measurements. It is a multiplicative calibration error, associated with some point estimators for shear in the presence of noise, such as a maximum likelihood estimate or expectation value for the ellipticity of a galaxy (Hirata et al. 2004; Refregier et al. 2012; Melchior & Viola 2012; Miller et al. 2013). Averaging these point estimators gives a biased estimate of the shear, and the bias remains even when response terms are included, such as that introduced by Kaiser et al. (1995) and Bernstein & Jarvis (2002).

For galaxy images with signal-to-noise ratio (S/N) ~ 10, the noise bias can be of order 10% for galaxies with size comparable to that of the point-spread-function (PSF). This multiplicative error is significantly larger than the requirements for current and planned surveys, which are $\sim$0.4% and $\sim$0.2%, respectively (Huterer et al. 2006).

A number of approaches have been proposed to address noise bias. I do not wish to give an exhaustive list, but rather a few examples.

A Bayesian approach to shear estimate was proposed by Miller et al. (2007) specifically to address noise bias. With that method, a point estimator for the shear is still used (the expectation value of the galaxy ellipticity), but a response term is calculated based on prior information of the true distribution of galaxy ellipticities and the likelihood surface for a given galaxy. A limitation of this method is that no expression was derived for the mean shear from an ensemble of galaxies, rather it was proposed to average the responses from individual galaxies. This method performs well in comparison to many previous methods, but does not meet the requirements for current and planned surveys (Bernstein & Armstrong 2014).

Zuntz et al. (2013) propose to use a point estimate from galaxy shapes and simply calibrate the answer using simulated data. A related idea has been proposed in schematic form by Refregier & Amara (2013), to use an iterative approach where the universe is simulated and its parameters tuned, along with calibration parameters of the measurement, to reproduce the observed results. These methods are in principle limited only by the accuracy of the simulations to represent the real universe.

A rigorous Bayesian formalism was developed by Bernstein & Armstrong (2014), hereafter BA14, that has the potential to recover shear with good accuracy using even very low S/N galaxy images. Rather than relying on a point estimate for the shear, they derived an expression for the mean shear estimated from an ensemble of measurements, exploiting the fact that the posterior for the shear must approach a Gaussian for a large

⋆ E-mail: erin.sheldon@gmail.com

ensemble. No corrections based on simulations are required. They showed that the method is sufficiently unbiased for current and planned surveys in a simple demonstration with galaxy ellipticities only, but no implementation for use with galaxy images was presented.

Here I present a full model-fitting implementation of the BA14 algorithm that works on galaxy images, including the effects of the PSF and pixelization. I test the implementation using a set of image simulations with idealized galaxy models, and show that in these controlled conditions the method is sufficiently accurate for current and planned surveys.

Below I follow the notation of BA14, where a shear was represented by the glyph $\boldsymbol{g}$.

2 ALGORITHM

Here I will give a brief overview of the method presented by BA14. There are two important assumptions underlying this approach (following the notation in BA14):

- The shear is weak, $\boldsymbol{g} \ll 1$.
- The posterior distribution of the mean shear derived from a large ensemble of galaxy images is approximately Gaussian.

The assumption of small shear is true in many circumstances, but breaks down along lines-of-sight near large over-densities, such as clusters of galaxies.

The second assumption follows from the central limit theorem: if the shear is derived from a large enough ensemble of galaxy shapes, the posterior approaches a Gaussian.

Note no assumptions are made about the likelihood surface for parameters derived for individual galaxies; only the ensemble average shear from a population can be assumed to follow a simple Gaussian distribution.

No information is necessarily "lost" by restricting shear estimation to populations rather than individual galaxies. Galaxies have intrinsic shapes that are a large effective noise for shear measurement, an order of magnitude larger than the signal. Thus some kind of averaging must be performed to extract a shear from galaxy shapes.

Given the above assumptions, the authors of BA14 derived a second-order Taylor expansion of the logarithm of the shear posterior about zero shear, consistent with the Gaussian assumption:

$$\begin{aligned} -\ln P(\boldsymbol{g}|\boldsymbol{D}) \quad &\approx \quad (\text{const}) - \ln P(\boldsymbol{g}) \\ &\quad -\boldsymbol{g} \cdot \sum_i \frac{\boldsymbol{Q}_i}{P_i} \\ &\quad +\frac{1}{2}\boldsymbol{g} \cdot \left[\sum_i \left(\frac{\boldsymbol{Q}_i \boldsymbol{Q}_i^T}{P_i^2} - \frac{\mathbf{R}_i}{P_i}\right)\right] \cdot \boldsymbol{g}, \end{aligned} \tag{1}$$

where $\boldsymbol{D}$ is the data vector and $\boldsymbol{g}$ is the two-component shear. The terms P_i, $\boldsymbol{Q}_i$, and $\mathbf{R}_i$ are

$$\begin{aligned} P_i &= P(\boldsymbol{D}_i|\boldsymbol{g}=0) \\ \boldsymbol{Q}_i &= \boldsymbol{\nabla}_{\boldsymbol{g}} P(\boldsymbol{D}_i|\boldsymbol{g})|_{\boldsymbol{g}=0} \\ \mathbf{R}_i &= \boldsymbol{\nabla}_{\boldsymbol{g}} \boldsymbol{\nabla}_{\boldsymbol{g}} P(\boldsymbol{D}_i|\boldsymbol{g})|_{\boldsymbol{g}=0}\,. \end{aligned} \tag{2}$$

P is the Bayesian "prior", and functionally corresponds to the true distribution of all the relevant galaxy parameters in the absence of shear. Note the prior on the shear $P(\boldsymbol{g})$ is assumed to be uninformative.

Accurate prior information for the galaxy shapes is important for this method: the derivatives of the un-lensed distribution of shapes with respect to shear encodes how the ensemble of galaxy images responds to a shear. With knowledge of the true population of shapes, and how that population transforms under shear, one can infer the applied shear, even in the presence of noise.

To predict the observed distribution of shapes in general, the un-lensed distribution of shapes must be mathematically sheared and compared to observables. However in the approximation given above, only derivatives near $g = 0$ are required and the mean shear $\bar{\boldsymbol{g}}$ and covariance matrix $\mathbf{C}_g$ can be found directly:

$$\begin{aligned} \mathbf{C}_g^{-1} &= \sum_i \left(\frac{\boldsymbol{Q}_i \boldsymbol{Q}_i^T}{P_i^2} - \frac{\mathbf{R}_i}{P_i}\right) \\ \bar{\boldsymbol{g}} &= \mathbf{C}_g \sum_i \frac{\boldsymbol{Q}_i}{P_i}. \end{aligned} \tag{3}$$

In practice the parameters of each galaxy are not precisely known. In that case the derivatives in equation 2 can be averaged over the full likelihood surface for each galaxy, taking care to use the prior distribution given the shear. These mean values can then be used in the aggregates shown in Equation 3.

A conceptual outline for measurement of non-constant shear was also given by BA14, as were third-order tweaks to the second-order perturbations.

A full implementation, fitting to pixelized galaxy images, was not attempted in BA14. The basic formalism was shown to work by drawing shapes randomly from an analytic distribution, adding noise and a small shear, and recovering that shear using second-order formula.

3 SIMULATION

In the absence of an absolute calibration source for weak lensing, some confidence in a shear measurement technique can still be derived using simulation. The Third Gravitational Lensing Accuracy Testing challenge (GREAT3, Mandelbaum et al. 2013) provides an excellent set of simulations for testing shear measurement methods. However, all the provided simulations include relatively realistic PSF and galaxy properties, features which can introduce additional errors beyond noise bias. Going forward, such simulation efforts will be important, but for this preliminary work I sought more controlled conditions.

I simulated elliptical Sérsic (Sérsic 1963) profiles to represent galaxies. The Sérsic profile for a round model is given by

$$I(r) \propto \exp\left[-\left(\frac{r}{r_0}\right)^{1/n}\right]. \tag{4}$$

For fixed n, the full elliptical model has six parameters: two centroid parameters, two ellipticity parameters, a size parameter and an amplitude, or flux parameter. I used two distinct values of the index: $n = 1$ (exponential disks), and $n = 4$ (De Vaucouleurs' profiles).

I simulated pairs of galaxy images with identical structural parameters, but with position angles offset by 90 degrees, in order to cancel the intrinsic shape noise. This simulation strategy is known as a "ring test"(Nakajima & Bernstein 2007). Using a ring test greatly reduces the number of simulated images required to reach a desired precision in the recovered shear.

I convolved the models with a round Gaussian PSF with $\sigma = \sqrt{2}$ pixels. I chose a Gaussian to minimize PSF modeling

errors, and made it round to avoid the potential additive bias associated with a non-circular PSF. I then convolved the models with a uniform square pixel response function.

For consistency, I chose the same un-lensed shape distribution used in Bernstein & Armstrong (2014):

$$P_0(e^s) \propto \left[1-(e^s)^2\right]^2 \exp\left[-(e^s)^2/2\sigma^2_{\rm prior}\right], \qquad (5)$$

with $\sigma_{\rm prior} = 0.3$. This distribution is sufficiently similar to the distribution of true galaxy shapes to be useful in this test. This distribution also has the required property that it is twice differentiable.

I drew the other galaxy parameters from simple non-covariant distributions. I drew the size parameter from a log-normal distribution with 30% scatter. The mean of the size distribution was chosen such that the average galaxy image had *observed, post-PSF* full-width at half maximum (FWHM) approximately 1.2 times that of the PSF. Due to the log-normal scatter, some galaxies were smaller and some larger.

I ran multiple simulations with different mean signal-to-noise ratios $(S/N)_{\rm matched}$ in the range $[10, 1000]$. Fluxes were drawn from a log-normal distribution and Gaussian noise was added so that the mean galaxy image had the desired $(S/N)_{\rm matched}$. The optimal, matched signal-to-noise ratio $(S/N)_{\rm matched}$ is defined as

$$(S/N)^2_{matched} = \frac{1}{\sigma^2_{sky}} \int I^2(x,y) dx dy \qquad (6)$$

where $I(x,y)$ is the true light profile and σ^2_{sky} is the variance of the Gaussian noise. This matched filter signal-to-noise can be shown to be the maximal possible measure of the signal-to-noise ratio, and was used as the signal-to-noise ratio definition for the GREAT08 and GREAT3 shear measurement challenges (Bridle et al. 2010; Mandelbaum et al. 2013). Other measures of S/N can be lower by as much as a factor of two (Mandelbaum et al. 2013).

By drawing sizes and fluxes from log-normal distributions I was attempting to very roughly approximate a selection that might occur in real data, for example binning galaxies by a robust flux measure such as a PSF flux and performing star-galaxy separation. Within a PSF flux bin, the true distribution of flux would have a small tail to lower values due to noise and a long tail to higher flux because galaxies can be larger than the PSF, causing the PSF flux to in some cases be an underestimate. By tuning the mean FWHM of the galaxies to be approximately 1.2 times that of the PSF, I was attempting to mimic the sort of noisy size cut that can occur when separating stars from galaxies at low signal-to-noise ratio.

Finally, I drew the centroid from a Gaussian in each coordinate, with σ of 0.1 pixels.

4 IMPLEMENTATION

As described in §2, in the presence of noise the estimator involves integrals of P, $\boldsymbol{Q}$ and $\mathbf{R}$ over the full likelihood surface for each galaxy.

Exploration of the likelihood surface in a high-dimensional space requires a large number of model evaluations, so I found efficiency to be important. As an optimization, I approximated galaxy models as sums of Gaussians according to the fits in Hogg & Lang (2013). I also fit the PSF using a Gaussian. Using Gaussians for both galaxy and PSF models facilitated performing fast analytic convolutions. This is a fast and simple alternative to convolutions using Fourier transforms.

By using a fit to the observed, pixelized PSF to convolve the galaxy models, I accounted approximately for the convolution by the pixels in the PSF model itself. This worked well for the parameters I used, but for a poorly sampled PSF this approach could result in relatively large errors.

I used a fast approximation to the exponential function for evaluating the Gaussians in the galaxy models. Even so, evaluation of the exponential function was the computational bottleneck for the likelihood evaluation.

I applied priors for the non-shape parameters in order to make exploration of the likelihood surface more efficient. The prior on the shapes was not applied during exploration, because the P, $\boldsymbol{Q}$ and $\mathbf{R}$ are to be averaged over the likelihood. This separation was possibly only because the shapes were not covariant with the other parameters.

During fitting, I used prior distributions matched exactly to the true distributions used in the simulation. I used the correct Sérsic index for fitting in each case; i.e. when simulating exponential disks, I also fit an exponential disk ($n = 1$). By choosing the true priors and model family, I tested the accuracy of the algorithm and likelihood sampling technique directly and avoided confusion with other issues such as model bias or empirical prior determination.

I used a Markov Chain Monte Carlo (MCMC) to explore the likelihood surface. I found using a standard Metropolis-Hastings algorithm (Metropolis et al. 1953) challenging because galaxies have a wide variety of best-fit model parameters and errors in those parameters, depending on the noise level. I did not find it straightforward to predict what the parameter errors would be a priori, which made it difficult to choose a "step size" for the MCMC chain. This is one reason I used an affine invariant MCMC (Goodman & Weare 2010). An affine invariant MCMC is dynamically adapted to the underlying distribution by comparing multiple "walkers" as they are moved through the parameter space; it thus does not require tuning the step size. I used the implementation presented in Foreman-Mackey et al. (2013) for this work.

For the MCMC I used an affine parameter $a = 2$, which gives an acceptance rate of about 0.5. I used 80 "walkers" in the chain, with 400 initial steps per walker for burn-in followed by 200 additional steps per walker for measuring expectation values. I found that increasing the number of steps generally resulted in less bias in the recovered shear, but I found diminishing returns beyond 200 for the simple models I was fitting.

I chose initial locations for the walkers to be centered on the maximum likelihood solution found with a Levenberg-Marquardt method (Levenberg 1944). The location for each walker was chosen from a multi-dimensional Gaussian centered at the maximum likelihood with scatter based on errors in the fit, truncated to positive for flux and size and within $(-1, 1)$ for shapes. I also tried centering the initial positions on the true parameters, as well as drawing the initial positions from the priors. All methods gave consistent results. For the large number of burn-in steps that I used the result was rather insensitive to the starting position.

It may be worth while to further optimize the exploration of the likelihood surface in terms of the number of walkers and steps used, but also the type of computing resources used. Graphics processing units may prove particularly useful; in a preliminary study I found an decrease in time per likelihood evaluation of order 100 over traditional processors.

As I will show in section 5.1, the formulas in BA14 break down at high shear. However, it is beneficial to perform tests at high shear because the number of simulated galaxies required to reach a specified fractional noise in the measured shear goes roughly as the inverse square of the shear. For this reason I chose to expand about the true shear instead of zero shear in Equations 1 and 2. I

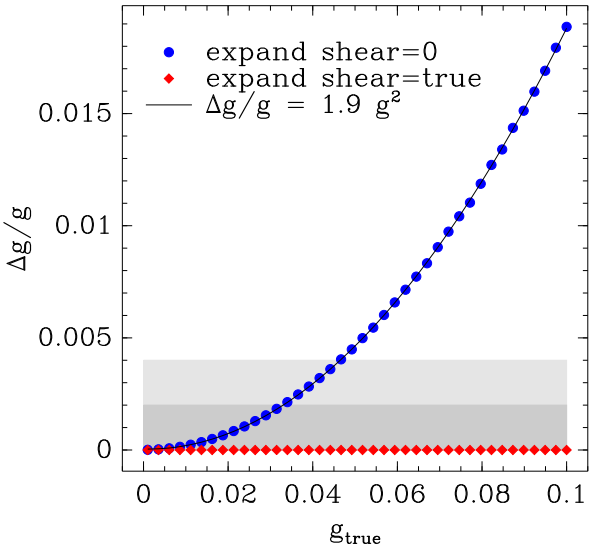

Figure 1. Fractional bias in the recovered shear $\Delta g/g = g/g_{true} - 1$ as a function of true shear, in a zero noise simulation. The blue circles represent the recovered shear when using the posterior equations expanded to second order about zero shear. The red diamonds represent expansion about the true shear. The solid curve represents the best-fitting quadratic function of the true shear $\Delta g/g \sim 1.9\, g^2_{true}$. The quadratic bias as a function of true shear indicates a break down of the second-order Taylor approximation presented in Bernstein & Armstrong (2014). The light and dark gray bands represent the approximate requirements for current and planned surveys respectively.

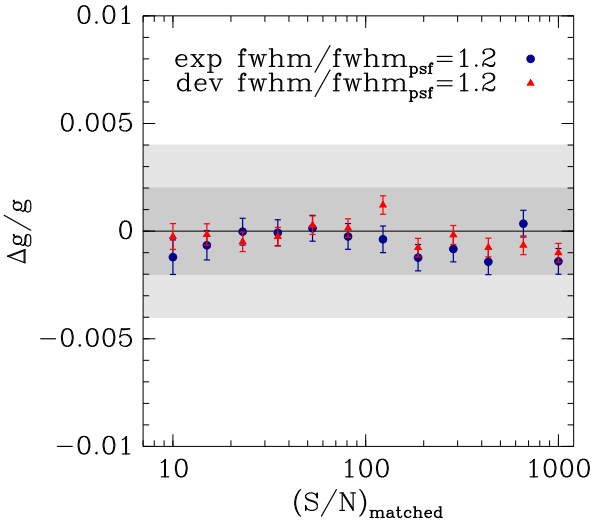

Figure 2. Fractional bias in the recovered shear for the estimator presented in Bernstein & Armstrong (2014). The bias is plotted as a function of the maximal, matched galaxy signal-to-noise ratio $(S/N)_{\rm matched}$, for galaxies with exponential (Sérsic $n = 1$) and De Vaucouleurs' profiles ($n = 4$). The simulated galaxy parameters were drawn from broad distributions in size, flux, and ellipticity. The size distribution was log-normal with 30% scatter and mean such that the *observed, post-PSF* FWHM was approximately 1.2 times that of the PSF, mimicking small galaxies that may pass a size cut, such as that used during star-galaxy separation. The flux distribution was log-normal with 30% scatter, and noise chosen to produce the indicated $(S/N)_{\rm matched}$. The ellipticities were drawn from the simple distribution introduced in Bernstein & Armstrong (2014). In these controlled conditions, this shear estimator meets the approximate accuracy requirements for current and planned surveys, shown as the light and dark gray bands, respectively.

also performed a more limited range of tests expanding about zero shear and shearing the images by $g = 0.01$, and got consistent results.

The code is freely available for download[1]. Potential users should note that, at the time of writing, the code is under heavy development and the application programming interface may evolve rapidly.

5 RESULTS

5.1 Calibration Bias vs. True Shear

Figure 1 contains results for a zero-noise simulation. The fractional bias is shown as a function of true shear. The bias is well fit by a quadratic function of the true shear, represented by the overlaid curve. This quadratic error is expected for a second-order Taylor expansion.

Because of this bias, I expanded the equations about the true shear rather than zero shear, as explained in §4.

5.2 Calibration Bias vs. Galaxy Signal-to-noise Ratio

Figure 2 contains the fractional error in the recovered shear as a function of optimal, matched signal-to-noise ratio $(S/N)_{\rm matched}$, for the simulated galaxies described in the previous sections. In these controlled conditions this implementation is unbiased at the $\Delta g/g \sim 2 \times 10^{-3}$ level.

The errors for the different values of $(S/N)_{\rm matched}$ appear to be correlated. This may be due to the details of how the likelihood surface was explored, and may be correctable by tuning the parameters of the affine-invariant MCMC chain, such as number of walkers, burn-in, or post-burn-in steps.

5.3 Comparison with Requirements for Current and Planned Surveys

In the figures above I showed gray bands representing the approximate multiplicative bias requirements for current surveys such as the Dark Energy Survey (DES Collaboration 2005, DES) and the Hyper-Suprime-Cam survey (Miyazaki et al. 2012, HSC), and planned surveys such as the Large Synoptic Survey Telescope survey (Ivezic et al. 2008, LSST) and the Euclid Mission (Laureijs et al. 2011). These requirements are based on the calculations presented by Huterer et al. (2006). I assumed fiducial sky coverage and that shear calibration bias results in less than 20% degradation in the accuracy of the recovered dark energy equation of state parameter relative to shot noise errors. The cut at 20% is somewhat arbitrary, and was chosen to coincide very roughly with the stated requirements for DES. The requirements are $\sim 4 \times 10^{-3}$ for current surveys and $\sim 2 \times 10^{-3}$ for planned surveys. These requirements are met in all the cases that I tested.

Smaller and fainter galaxies might have more bias than the average. The authors of Bernstein & Armstrong (2014) noted that small and faint galaxies, for which the ellipticity likelihood is broad, get little weight in the average shear measurement relative to larger and brighter galaxies. This is an intrinsic feature of the estimator, no additional weighting is needed. Indeed I made no cuts

[1] https://github.com/esheldon/ngmix

on the simulated galaxies used for this measurement, even though some had signal-to-noise ratio much less than 10, yet I recovered the shear with good accuracy. This is a useful property of the estimator, as the shear measurement process need not necessarily introduce additional selection effects.

In Figure 1 I showed the multiplicative bias due to the breakdown of the second-order Taylor expansion at higher shear. This effect is prohibitive for current surveys when the shear exceeds 0.05. The authors of BA14 suggested potentially using higher order information to tweak the second order equations. I have not yet explored that approach.

6 DISCUSSION

The success of this implementation in a controlled simulation is strong encouragement for further development of this method. However, the model-fitting approach I presented here may ultimately only be useful as a proof-of-principle: model-fitting is limited by the accuracy of the models to represent true galaxies, and thus in real data additional errors will be present; this is the so-called "model bias".

Kacprzak et al. (2013) showed that model bias may be on the order of baseline requirements for current surveys, but potentially crippling for future surveys with more stringent requirements. One potential solution is to fit models with more freedom. However, fitting a more complex model often results in a more complex likelihood surface. To fully explore the surface requires more burn-in for an MCMC chain and more samples to estimate the expectation values for the P, $\boldsymbol{Q}$ and $\mathbf{R}$ parameters. I leave tests with more complex models to future work.

As an alternative to model fitting, Bernstein & Armstrong (2014) propose to measure moments in Fourier space, making no explicit parameterization of galaxy light distributions beyond the observed pixel values. The moments are interpreted using a Bayesian formalism similar to that used for model fitting, and so could be robust to noise bias effects. Evaluation of this Fourier method in the presence of noise is worthy of future effort.

ACKNOWLEDGMENTS

ES is supported by DOE grant DE-AC02-98CH10886.

Thanks to Gary Bernstein, Bob Armstrong, Jim Bosch, Mike Jarvis and Robert Lupton for many useful discussions; thanks to Anže Slosar for suggesting I expand the equations about the true shear to reduce the number of simulated images required for each test. Thanks to the STAR, PHENIX and LBNE experiments at BNL for use of spare cycles on their compute clusters, and to the staff of the Rhic Atlas Computing Facility at BNL for their continued, and disproportionately large support of my work.

REFERENCES

Bernstein G. M., Armstrong R., 2014, MNRAS, 438, 1880
Bernstein G. M., Jarvis M., 2002, AJ, 123, 583
Bridle S., et al., 2010, MNRAS, 405, 2044
DES Collaboration 2005, ArXiv:astro-ph/0510346
Foreman-Mackey D., Hogg D. W., Lang D., Goodman J., 2013, PASP, 125, 306
Goodman J., Weare J., 2010, App. Math. Comp. Sci., 5, 65
Hirata C. M., et al., 2004, MNRAS, 353, 529
Hogg D. W., Lang D., 2013, PASP, 125, 719
Huterer D., Takada M., Bernstein G., Jain B., 2006, MNRAS, 366, 101
Ivezic Z., et al., 2008, ArXiv e-prints
Kacprzak T., Bridle S., Rowe B., Voigt L., Zuntz J., Hirsch M., MacCrann N., 2013, ArXiv e-prints
Kaiser N., Squires G., Broadhurst T., 1995, ApJ, 449, 460+
Laureijs R., et al., 2011, ArXiv e-prints
Levenberg K., 1944, Quarterly of Applied Mathematics, 2, 164
Mandelbaum R., et al., 2013, ArXiv e-prints
Melchior P., Viola M., 2012, MNRAS, 424, 2757
Metropolis N., Rosenbluth A. W., Rosenbluth M. N., Teller A. H., Teller E., 1953, J. Chem. Phys., 21, 1087
Miller L., et al., 2013, MNRAS, 429, 2858
Miller L., Kitching T. D., Heymans C., Heavens A. F., van Waerbeke L., 2007, MNRAS, 382, 315
Miyazaki S., et al., 2012, in Society of Photo-Optical Instrumentation Engineers (SPIE) Conference Series Vol. 8446 of Society of Photo-Optical Instrumentation Engineers (SPIE) Conference Series, Hyper Suprime-Cam
Nakajima R., Bernstein G., 2007, AJ, 133, 1763
Refregier A., Amara A., 2013, ArXiv e-prints
Refregier A., Kacprzak T., Amara A., Bridle S., Rowe B., 2012, MNRAS, 425, 1951
Sérsic J. L., 1963, Boletin de la Asociacion Argentina de Astronomia La Plata Argentina, 6, 41
Zuntz J., Kacprzak T., Voigt L., Hirsch M., Rowe B., Bridle S., 2013, MNRAS, 434, 1604